

The Tolman Surface Brightness Test for the Reality of the Expansion. II. The Effect of the Point-Spread Function and Galaxy Ellipticity on the Derived Photometric Parameters

Lori M. Lubin^{1,2}

*Department of Astronomy, California Institute of Technology,
Mailstop 105-24, Pasadena, California 91125*

Allan Sandage

*Observatories of the Carnegie Institution of Washington,
813 Santa Barbara Street, Pasadena, California 91101*

ABSTRACT

To complete the Tolman surface brightness test on the reality of the expansion of the Universe, we need to measure accurately the surface brightness profiles of the high-redshift galaxy sample. To quantify this accuracy, we investigate the effects of various sizes of point-spread functions composed of telescope diffraction, CCD pixel resolutions, and ground-based seeing on the measurements of mean surface brightness for galaxies whose effective (half-light) radii range from $0''.70$ to $0''.17$. We have done the calculations using two synthetic galaxies of effective radii of $0''.70$ and $0''.25$ with point-spread functions of 0.1, 0.3, and 0.9 arcseconds, full width at half maximum. We have also compared actual observations of three high-redshift galaxies in the cluster Cl 1324 + 3011 ($z = 0.76$) made both with the ground-based Keck 10-m telescopes in seeing of about $0''.9$ and with the *Hubble Space Telescope* (HST) with a point-spread function that is approximately ten times smaller. The conclusion is that HST data can be used as far into the galaxy image as a Petrosian metric radius of $\eta = 1.3$ magnitudes, whereas the ground-based data will have systematic errors of up to 2.9 magnitudes in the mean surface brightness at η values of less than 2.2 magnitudes for all but the largest galaxies at redshifts of $z \approx 0.7$.

In the final section, we compare the differences in derived average surface brightness for nearly circular galaxy images compared with highly flattened images. The comparison is made by using the two reduction procedures of (1) integrating the profile curves using circular apertures, and (2) approximating an “equivalent circular” galaxy that is highly elongated by using an “effective” radius of \sqrt{ab} , where a and b are the semi-major and semi-minor axis, respectively, of the best-fitting ellipse. The conclusion is that the

¹Hubble Fellow

²Current address : Department of Physics and Astronomy, Johns Hopkins University, Baltimore, MD 21218

two methods of reduction give nearly identical results and that either method can be used to analyze the low and high-redshift galaxy samples used in the Tolman test.

Subject headings: galaxies: clusters: general – cosmology: observations

1. Introduction

More than seventy years ago, Tolman (1930, 1934) showed that, in an expanding universe with any arbitrary geometry, the surface brightness of a set of "standard" (identical) objects will decrease with redshift as $(1+z)^4$. In this series of papers, we present the necessary steps to carry out the Tolman test using early-type galaxies which are members of three high-redshift clusters, Cl 1324+3011 at $z = 0.76$, Cl 1604+4304 at $z = 0.90$, and Cl 1604+4321 at $z = 0.92$ (Oke, Postman & Lubin 1998; Postman, Lubin & Oke 1998, 2001; Lubin et al. 1998, 2001). In the first paper in this series (Sandage & Lubin 2001; hereafter Paper I), we discussed the validity of the Tolman test, described how we will use the observed photometric properties of early-type galaxies to measure the surface brightness dimming as a function of redshift, and calibrated the correlations between average surface brightness, absolute magnitude, and linear radius for the local galaxy sample. To use the fiducial (zero redshift) relations derived in Paper I, we need to measure the same observable parameters in our high-redshift galaxy sample. The purpose of this paper is to explore possible errors in measuring these parameters from CCD imaging and to determine how these uncertainties might affect the Tolman test.

First, we quantify the systematic errors in the determination of Petrosian (1976) η radii caused by a finite point-spread function (PSF) from telescope diffraction, CCD pixel size, and the atmospheric seeing disk if the observations are made from the ground. The Petrosian η radius function is defined as the difference in magnitude between the mean surface brightness, $\langle SB(r) \rangle$, averaged over the area interior to a particular radius and the surface brightness, $SB(r)$, at that radius. This function is discussed in §2 of Paper I where some of its unique properties in defining a metric size are described.

While other authors have examined how seeing affects certain photometric properties of elliptical galaxies (e.g. Schweizer 1979, 1981; Sparks 1988; Saglia et al. 1993), we need to determine specifically the sensitivity of $\eta(r)$ to the size of the PSF. We have done this in two ways. (1) Simulations using an assumed true intensity profile are folded with different PSFs to give a family of "observed" profiles that are then used to derive the other photometric parameters. (2) The derived η radii for a sample of galaxies that have been observed with both the Keck 10-m telescopes and the *Hubble Space Telescope* (HST) which has a PSF about ten times smaller are compared. The results of the simulations are given in §2 for the effect on the measured photometric parameters of four assumed PSF widths for two galaxies of different half-light angular radii. In §3 we show the comparisons using actual data for three early-type galaxies at high redshift observed both from the ground with Keck and from space with HST by Postman et al. (1998, 2001) and Lubin et al. (1998,

2001).

Second, we show in §4 the effects on $\eta(r)$ of using elliptical-aperture photometry on highly elongated early-type galaxies and defining the photometric parameters from the resulting intensity profile as a function of the effective radius, \sqrt{ab} , where a and b are the semi-major and semi-minor axes, respectively, of the best-fitting ellipse. We investigate how well the integration using circular symmetry of an \sqrt{ab} profile agrees with the pixel-by-pixel summing in circular apertures of the actual two-dimensional observed surface brightness array of the same galaxies.

2. The Effect of Various Point Spread Functions on the Measured Photometry Parameters by Simulations

To assess the effects of finite point-spread-functions on measurements of (1) mean surface brightness, (2) total magnitude, and (3) metric radius at particular Petrosian η values, we have simulated observations of two elliptical galaxies with seeing and point-spread functions whose total widths at half maximum vary from zero to $0''.9$. We have chosen the size of the intrinsic galaxy profiles for the simulations to match closely two galaxies from the cluster Cl 1324 + 3011 at $z = 0.76$ that are included in the sample of high-redshift, early-type galaxies in Lubin & Sandage (2001a; hereafter Paper III).

For the first galaxy we choose HST #9 in Cl 1324 + 3011 which is classified as an elliptical and which is the first-ranked cluster member both in apparent magnitude and in angular size. The total I magnitude on the Cape/Cousins photometric system is $I = 19.85$. The effective (half-light) radius is $0''.70$, as determined from the HST image (Lubin et al. 2001). This is 7 pixels on the pixel scale of $0''.0996$ per pixel for the Wide Field Planetary Camera 2 (WFPC2) chips. The second galaxy for the simulation is the much fainter and smaller elliptical cluster member, HST #59, whose total magnitude is $I = 22.09$ and whose effective radius is $0''.25$. For the simulation we model the surface brightness profile of each galaxy by a de Vaucouleurs $r^{\frac{1}{4}}$ law as

$$I = I_o \exp \left[-7.67 \left(r/r_{eff} \right)^{\frac{1}{4}} \right]. \quad (1)$$

For both simulated galaxies we assume a circular image and perform the necessary integrations for the mean surface brightness, growth curve, and Petrosian η radii using circular-aperture integration over the synthetic galaxy images.

2.1. The Galaxy Simulations

The artificial galaxies were created using the IRAF task MKOBJECTS. This program allows us to create the galaxy profile, convolve it with a seeing disk and/or PSF, add the sky background, and add Poisson noise. For these simulations, we have first chosen a simple representation of the

seeing and have modeled the PSF as a Gaussian; however, we also explore the effect of the more complicated PSF of the WFPC2 on the HST observations (see §2.2).

For the intrinsic case of no seeing and zero width to the PSF, we have simulated the galaxy profiles with a pixel scale of $0''.010$ per pixel. This resolution is ten times better than that assumed for the WFPC2 in the finite seeing/PSF simulations. For the calculation of the intrinsic profile, a calculation grid as defined by a pixel scale, no matter how small, is necessary. However, we have made the pixel scale small enough so that the width of the intrinsic profile is effectively zero to an excellent approximation.

For the cases where we include seeing and the PSF at various levels, we simulate the 32 ksec HST observation of Cl 1324 + 3011 (Lubin et al. 2001) by using the appropriate pixel scale of $0''.0996$ per pixel and including the same background level (272 DN) of the WFPC2 observations taken in the F814W filter, which closely resembles the *I* band. In addition, we have added Poisson noise using the gain and read-noise parameters of the WFPC2 which are $7 \text{ e}^-/\text{DN}$ and 5 e^{-1} , respectively. To add the effect of seeing, we have convolved the galaxy profiles with a Gaussian profile with major axis, half-intensity diameters of 0.1, 0.3, and 0.9 arcsec, respectively. The profiles of the two artificial galaxies, convolved by the adopted family of PSF functions and with the noise sources added as described above, were then used to calculate the resulting “observed” parameters of (1) the surface brightness profiles, (2) the growth curves for the total magnitude, and (3) the Petrosian η values at various angular radii. These functions are calculated using the profile-fitting IRAF task ELLIPSE, assuming circular aperture integrations.

Curves of these functions are given in Figures 1 and 2 for HST #9 and #59, respectively. The solid (red) curves in each panel represent the “no seeing” case. We adopt these as the intrinsic profiles for the two galaxies. The “observed” curves for the three parameters of profile, growth curve, and $\eta(r)$ are shown for the three finite seeing PSFs. The key for these curves are marked in the panel for the η function. The PSF of $0''.1$ (full width at half maximum) resembles the level that can be obtained with HST, while the seeing of $0''.9$ is typical of observations using the Low Resolution Imaging Spectrograph (LRIS; Oke et al. 1995) on the Keck 10-m telescopes.

The conclusion that will be important for the Tolman test in Lubin & Sandage 2001b (hereafter Paper IV) concerns the accuracy with which the η radii can be determined with HST given its PSF of about $0''.1$. For the larger of the two simulated galaxies HST #9, the intrinsic η profile is reached (to within 5%) at $\eta = 1.1$ where $\log r = -0.40$ (or $r = 0''.40$) for the $0''.1$ seeing case. The intrinsic η of the $0''.3$ seeing case for this galaxy is not reached until $\eta = 1.6$ at $\log r = 0.04$ (or $r = 1''.10$). For the case of $0''.9$ seeing (equivalent to the Keck observations), the intrinsic η is not reached until $\eta = 2.2$, at which place the angular radius is $2''.39$. The situation, of course, is more severe for the smaller galaxy, HST #59. For the $0''.1$ seeing case, the intrinsic η is reached (to within 5%) only at $\eta = 1.6$ at which point the angular radius is $0''.40$. For the $0''.9$ (ground-based) seeing case, the true η curve is reached only at large angular radii where $\eta > 2.5$.

The systematic error on the surface brightness averaged over the η radii, i.e. $\langle SB \rangle$, is seen by

reading the growth curves at these radii. For the case of the $0''.1$ PSF, the intrinsic growth curve of HST #9 has been reached to within the 0.02 magnitude level by $\log r = -0.40$ (or $\eta = 1.1$). Hence, because the observed η values for the $0''.1$ seeing have also been reached by $\eta = 1.1$ as discussed above, the $\langle SB \rangle$ values for galaxies which are the size of HST #9 (half-light radius of $0''.70$) will have no systematic errors in the $\langle SB \rangle - \eta(r)$ correlations for all η values greater than 1.1 mag. For the smallest galaxies in Cl 1324 + 3011, such as HST #59 whose half-light radius is $0''.25$, the systematic errors in $\langle SB \rangle$ due to the PSF of $0''.1$ will become negligible only for η values larger than 1.6 mag. This conclusion is seen in the same way as above by noting from Figure 2 that both the growth curve and the η curve have reached the intrinsic curves only by this η value.

2.2. The WFPC2 Point Spread Function

The simulations presented above provide us with a general picture of how seeing between $0''.1$ and $0''.9$ affects the galaxy profile. Unfortunately, instrument PSFs, in particular that of WFPC2, are considerably more complex. Although a Gaussian function represents well the seeing disk and the initial turndown of the PSF, the wings of the PSF typically have a shallower fall-off than a Gaussian, with a slope that is more similar to an inverse-square power law (e.g. King 1971; Kurst 1995).

To explore how the exact WFPC2 PSF will affect our results, we have used the program Tiny Tim by J. Kirst and R. Hook (see www.stsci.edu/software/timytim) to generate a representative PSF on the WFC chip 3 and in the F814W filter. We then convolve this PSF with the theoretical profiles of HST #9 and 59 (as described above) using the MKOBJECTS program. The results of these simulations are qualitatively similar to those of the Gaussian seeing; however, the larger extent of the actual PSF means that the HST profile reaches the intrinsic (no seeing) profile at larger radii. Specifically, the intrinsic η curve is reached (to within 5%) at $\eta = 1.3$ where the angular radius $r = 0''.7$ for the larger galaxy HST #9 and at $\eta = 1.8$ where $r = 0''.6$ for the smaller galaxy HST #59. At these respective η values, the error in the measured mean surface brightness $\langle SB \rangle$ is less than 0.07 mag. Consequently, there will be no systematic errors in $\langle SB \rangle$ for these η values or larger.

We will test these predictions in Paper IV for the three high-redshift clusters studied there by noting systematic differences in the Tolman signal that is determined from the mean surface brightness versus metric radius correlations using η values that range from 1.3 to 2.0 magnitudes.

3. Comparison of Photometric Parameters of Three Galaxies Observed With Both HST and the Keck 10-m Telescopes

In the three clusters to be used for the Tolman test in Paper IV, all galaxies with data from HST also have photometric data taken with LRIS on the Keck 10-m telescopes (Oke, Postman

& Lubin 1998; Postman, Lubin & Oke 1998, 2001; Lubin et al. 1998, 2001). In this section we compare the actual data obtained using HST with the ground-based data for three galaxies from the cluster Cl 1324 + 3011 at a redshift of $z = 0.76$.

Table 1 gives the characteristics of the three galaxies. The effective radii, as measured from the HST images, range from $0''.35$ to $0''.17$, all smaller than the effective radius for HST #9 with $r_{eff} = 0''.70$ described in §2. The smallest of the three galaxies, HST #69 with $r_{eff} = 0''.17$, is smaller than HST #59 with $r_{eff} = 0''.25$ which is also discussed in §2. The apparent magnitudes in I for the three galaxies range from 20.88 mag to 22.20 mag within a circular aperture of $3''$ in radius. These values closely match the asymptotic total magnitudes of the growth curves in Figures 3, 4, and 5. Both the HST and the Keck images of the three galaxies have been reduced in a manner similar to that described in §2. Here, however, we have fit elliptical apertures to the two-dimensional data so as to get the most accurate representation of the galaxy profile (see also §4). The resulting curves of surface brightness, total magnitude, and Petrosian radii η , which are shown in Figures 3 – 5, are plotted against $\log a$, where a is the semi-major axis of the best-fitting elliptical aperture. The curves are derived from data taken in the Cape/Cousins I band for the Keck observations and the F814W filter for the HST observations. The two bandpasses are very similar with $F814W = I + 0.05$.

Figure 3 shows the comparison for HST #18. It is the largest of the three galaxies and has photometric characteristics which are approximately the mean of the two galaxies presented in §2 and shown in Figures 1 and 2. The Keck η curve does not reach the equivalent HST η curve until $\eta \approx 2.2$. Therefore, the measured angular radii from the Keck data are too large compared to the true (HST) η value by factors that range from a factor of 2.2 at $\eta = 1$, decreasing to a factor of 1.7 at $\eta = 1.5$. Although the difference in the total magnitude between the HST and Keck profiles decreases with increasing radius, it is still 0.15 magnitudes too faint at a radius of $2''$. Hence, for galaxies with $r_{eff} = 0''.35$, no reliable mean surface brightness values can be obtained from ground-based data with the LRIS seeing level even at η values of 2. That is, the inferred $\langle SB \rangle$ values from the Keck ground-based data will be too faint by 1.7 mag at $\eta = 1$ and 1.3 mag at $\eta = 1.5$.

The situation becomes progressively worse, of course, as the effective radius decreases. Figure 4 shows the case for HST #40 with $r_{eff} = 0''.26$. Here, the HST η radius is never attained by the measured Keck $\eta(r)$ curve for any reasonable values of η . Figure 5 shows the case for $r_{eff} = 0''.17$ where the errors due to seeing are the worst of the three. At a fixed η value, the mean surface brightness is underestimated by up to 2.9 magnitudes when the Keck data are used to measure the profiles of these galaxies. The clear conclusion from these comparisons is that, for small galaxies, no reliable data on surface brightness can be obtained from ground-based observations with seeing of $0''.9$. Even for the largest galaxies at $z \approx 0.7$, only profile data at Petrosian radii values of $\eta > 2$ can be accurately used. This conclusion is, of course, not a surprise; however, it is here made quantitative.

It should also be noted that deconvolution methods can be used to recover the original galaxy

profile if the PSF of the instrument can be accurately measured. Such methods have improved considerably over the past years due to detailed analyses of images from WFPC and WFPC2 aboard the *Hubble Space Telescope*. For this project, we have chosen not to employ any deconvolution methods, but rather to use profile data only where we can be assured of the measurement accuracy. We have done this because the point-spread-functions of both the WFPC2 and the LRIS CCDs are a strong function of chip position. For example, the ellipticity of the PSF varies from 1% at the chip center to 15–25% at the chip edge (see e.g. Krist 1995; Hoekstra et al. 1998; Clowe et al. 2000; Squires et al. 2001). In addition, the PSF of the LRIS CCD is dependent on the rotator position. Consequently, the PSF as a function of chip position has to be measured separately for each LRIS image (Squires et al. 2001). Because we are analyzing galaxy profiles across the entire field for both the HST and Keck observations, we would need to measure the PSF at all chip positions. Since we have shown in §2 that the high-angular-resolution HST data is a reasonable measure of the true galaxy profile over the range of Petrosian radii in which we are interested ($\eta \gtrsim 1.3$), we have chosen to use the HST profiles without deconvolution.

4. Comparison of Photometric Parameters Measured With Circular Apertures on Highly Elongated Galaxies

4.1. Various Procedures for Reducing Photometric Data for Highly Elongated Early-Type Galaxies

A persistent problem in the photometry of galaxies is how to treat the photometric data to obtain Petrosian radii, mean surface brightness, and magnitudes inside given apertures for early-type galaxies that are highly elongated. In the methods of single aperture photoelectric photometry done between 1950 and 1980 before two dimensional array detectors were available, the focal plane blocking apertures at the telescope in the photometers were circular. The growth curves were obtained directly from the data as the sizes of the blocking apertures were increased. All of the aperture photometry and the growth curves in the literature of the 1970’s on the velocity-distance relation (e.g. Sandage 1972a,b,c; 1973) were made in this way.

When two-dimensional photoelectric data became available with the invention of areal detectors, a number of different decisions had to be made on how to present and to analyze the data. Among the many methods used in the presentation of the data are (1) to give the intensity profile (mag per arcsec² at a particular radii) along the major axis, listing the *semi-major axis* angular distances from the center, (2) the same profile as in (1) but listed using the “effective radius” defined as \sqrt{ab} for the best-fitting ellipse, or (3) an “effective profile” defined as the projection of the two-dimensional data onto the major axis and listed by semi-major axis angular distances (see Watanabe, Kodaira & Okamura 1982).

The growth curves of magnitudes versus radii can be obtained either by integrating the one-dimensional profile or by using the two-dimensional data in several ways. First, numerical aperture

photometry can be done by summing the intensities, pixel-by-pixel, in circular areas of growing size. This imitates the 1970’s growth curve observations made at the telescope with single-channel photometers using circular blocking apertures. Second, a more elaborate method is to fit elliptical isophotal contours to the two-dimensional data and to numerically sum the intensities using elliptical apertures. This procedure is equivalent to observations using a single channel photometer at a telescope by using different sized blocking diaphragms that would be elliptical to fit the galaxy contours. The resulting growth curve, plotted as a function of some measure of the angular radii, either the semi-major axis distance, a , or the “effective” radii, \sqrt{ab} (Lauer 1985). Third, an integration can be made of the profile data using any of the modes of presentation enumerated earlier using a circular-aperture assumption for the integration over an area. Generally, the results for the Petrosian metric radii $\eta(r)$, the average surface brightness $\langle SB \rangle$, and the growth curve will differ systematically among the methods.

All of these methods and more have been used in the literature, although sometimes there is insufficient information to tell which profile and which definition of angular radius is used. The purpose of this section is to make explicit the methods that we have used for Papers III and IV, as well as to compare these methods with those that are used in Paper I to make the local calibrations. Specifically, the data in Paper I were obtained from circular-aperture photometry on all of the local galaxies regardless of their ellipticity (see §3 of Paper I and below).

4.2. Comparison of Circular-Aperture Photometry With \sqrt{ab} Profile Photometry for Highly Elongated Galaxies

Postman & Lauer (1995) reduced their two-dimensional CCD photometry of the first ranked cluster galaxies in their sample of 119 Abell clusters by using circular-aperture integrations, pixel-by-pixel, from the two-dimensional image arrays. Their circular-aperture growth-curve magnitudes for various radii are listed in their Table 3. We have used these data in Paper I to define the zero redshift calibrations of the $\langle SB \rangle$, Petrosian radii $\eta(r)$, and growth-curve correlations. On the other hand, the correlations for the local calibrations used by Sandage & Perlmutter (1991a,b) to derive similar calibrations using independent data from the literature sources cited in Paper I were made by integrating profile data that were generally given as a function of the “effective” radius, \sqrt{ab} . That is, the surface brightnesses were measured along the semi-major axis, but the resulting surface brightness profile was listed as a function of radius $r = \sqrt{ab}$. This profile is often referred to as the “equivalent circular” galaxy that, to some degree, imitates a highly flattened galaxy. But how close is the correspondence?

To explore this correspondence, we compare in this section three different methods for analyzing the two-dimensional CCD images and calculate the resulting curves of surface brightness, total magnitude, and η . The three methods are as follows :

1. The two-dimensional data for the galaxy image are analyzed by using a series of circular

apertures, regardless of the ellipticity of the galaxy. The surface brightness profile (in mag per arcsec²) is measured at the circular radius r , and the growth curve is derived by summing the pixel intensities within each circular aperture.

2. The two-dimensional data for the galaxy image are fitted by a series of ellipses of progressively larger semi-major axis sizes. The surface brightnesses are measured along the major axis, and the growth curve is derived by summing the pixel intensities within each elliptical contour. The resulting parameters are listed against the semi-major axis a .
3. The tabulated surface brightness (SB) profile as measured in item (2) is used; however, it is plotted as a function of $r = \sqrt{ab}$ for the radii, instead of the semi-major axis, a . This profile is then re-integrated under a circular-aperture assumption as $\int SB \, 2\pi r dr$ in order to obtain the mean surface brightness, growth curve, and $\eta(r)$. This is said to approximate the same parameters of an “equivalent circular” galaxy.

In Papers III and IV, we shall use the \sqrt{ab} radii analysis (item 3) for the high-redshift cluster galaxies. However, the data which was used in Paper I for the fiducial (local) lines was reduced by Postman & Lauer (1995) with circular apertures placed on the observed two-dimensional array (item 1). For our analyses in Paper I, we did not need the profile data as the growth curves were all that were necessary to derive $\langle SB(\eta) \rangle$ and $\eta(r)$.

Since we are using two different data analysis methods for the Tolman test, it is essential to assess how well the $r = \sqrt{ab}$ “equivalent circular galaxy” assumption used in Papers III and IV agrees with the circular aperture reductions for highly elongated galaxies presented in Paper I. We have made the comparison using two galaxies in the cluster Cl 1324 + 3011 at a redshift of $z = 0.76$. The first galaxy HST #11 (Lubin et al. 2001) is nearly circular with an minor-to-major axis ratio of $b/a = 0.9$ near the center, flattening to $b/a = 0.75$ far from the center. The comparison galaxy is HST #12 which is highly elongated with an average minor-to-major axis ratio of $b/a = 0.50$. The detailed data on these galaxies, which are based on original data from Lubin et al. (2001), are set out in Paper III where all of the photometry for the Tolman-test clusters is listed.

Figures 6 and 7 show the digital images of HST #11 and HST #12 from the WFPC2 data which was taken in the F814W filter. Figures 8 and 9 show the diagnostic diagrams for HST #11 and #12 determined from the three methods described above. The solid blue circles show the results of the circular aperture analysis (item 1); the solid cyan squares represent the elliptical aperture analysis where the resulting curves are plotted against semi-major axis a (item 2); and the open red circles represent a re-analysis of the elliptical aperture data using the effective circular radius of \sqrt{ab} (item 3).

We first discuss Figure 8 which presents the results for the nearly circular galaxy of HST #11. As expected for a nearly round galaxy, all three curves in each panel give very consistent results for all radii except those in the very center (i.e. $\log r \lesssim -0.5$ or $\eta \lesssim 1$). In order to carry out the Tolman test, we must compare the low and high-redshift data using both the mean surface

brightness and the linear radius at a given η . Therefore, the two most crucial diagrams are $\langle SB \rangle$ versus η (lower right panel) and η versus radius (upper right panel). The conclusion is that for values of $\eta > 1$ all three methods give nearly identical results for the mean surface brightness at a given η . The average difference between all three methods is $\Delta\langle SB \rangle = 0.07$ magnitudes for all Petrosian radii with $\eta > 1$.

We note, however, that in the $\eta - \log r$ panel, even for the nearly circular galaxy HST #11, the curve derived using elliptical apertures (solid cyan squares) begins to deviate systematically from the other two curves at large η where the ellipticity is highest (i.e. $b/a = 0.75$). At $\eta > 1.4$, the average difference between the circular aperture and elliptical apertures method is $\Delta(\log r) = 0.10$ (a 26% error in r). However, this difference is only $\Delta(\log r) = 0.03$ (a 7% error in r) between the circular aperture and \sqrt{ab} methods. This is, of course, because the semi-major axis a is larger than the “equivalent circular” galaxy using the \sqrt{ab} approximation. Hence, even though the lower right panel shows near agreement in the $\langle SB \rangle - \eta$ plane at mid- η values, the systematic differences in the $\eta - \log r$ plane will cause a systematic difference in any comparison if one set of data would be reduced using the elliptical aperture (major axis) method, while another set would be reduced by either the circular aperture method or the closely equivalent \sqrt{ab} method.

These differences are, of course, larger for the highly elongated galaxy HST #12 in Figure 9. Here, the increased radius of the major axis method is well seen in the upper left panel of surface brightness (SB) versus \log (radius). However, as in Figure 8, the $\langle SB \rangle$ versus η panel at the lower right shows only a modest spread between the three methods for mid- η values. The average difference is $\Delta\langle SB \rangle = 0.13$ magnitudes for all Petrosian radii of $1 < \eta \leq 2$. Again, the important panel to consider is the $\eta - \log r$ panel at the upper right. While the elliptical aperture method is substantially different, the circular aperture (solid blue circles) and the \sqrt{ab} (open red circles) methods define nearly the same η curve to within 0.03 in $\log r$ for all radii with $\log r > -0.4$. This proves again that use of the \sqrt{ab} measure of the “effective” radius is closely equivalent to the use of circular-aperture photometry. We make use of this important conclusion in Papers III and IV in the discussion of the high-redshift cluster photometry.

5. Conclusions

In order to perform successfully the Tolman test using data from high-redshift cluster galaxies, we must make a reliable measure of the galaxy surface brightness profiles which are used to derive the essential parameters of mean surface brightness, total magnitude, and the Petrosian metric radius. In this paper, we have quantified the reliability of these quantities, first, by measuring the effect of seeing on the galaxy profiles and, second, by comparing the various methods of reducing the galaxy imaging data. Using both simulations of galaxy profiles convolved with Gaussian seeing from zero to $0''.9$ and actual data obtained with the *Hubble Space Telescope* and the Keck telescopes, we have found that high-angular-resolution data similar to that of HST can be used reliably to measure galaxy properties as far into the galaxy image as a Petrosian metric radius as small as $\eta \approx 1.3 - 1.8$,

depending on the angular size of the galaxy. On the contrary, ground-based data taken in poor seeing (full width at half maximum of $0''.9$) have systematic errors of up to 2.9 magnitudes in the mean surface brightness for all Petrosian metric radii with $\eta \lesssim 2.2$ for all but the largest galaxies at redshifts of $z \approx 0.7$.

While the imaging data on the local galaxies which will serve as our zero-redshift calibration for the Tolman test were originally analyzed using circular apertures, we have analyzed the CCD images of our high-redshift galaxy sample through the “equivalent circular galaxy” method which gives the surface brightness profile (measured in elliptical apertures) as a function of the effective radius, \sqrt{ab} . We have shown that both methods are consistent to within 7% for all Petrosian radii values of $\eta > 1$ for nearly circular galaxies, as well as highly elongated galaxies. Hence, the Tolman test is practical using these methods because an accurate comparison between the profile data of the low and high-redshift galaxy samples can be made.

We thank the anonymous referee for suggesting useful additions to this paper. We also thank Marc Postman and J.B. Oke for their permission to use part of their extensive Keck and HST database in this paper. LML is supported by NASA through Hubble Fellowship grant HF-01095.01-97A from the Space Telescope Science Institute, which is operated by the Association of Universities for Research in Astronomy, Inc., under NASA contract NAS 5-26555. AS acknowledges support for publication from NASA grants GO-5427.01-93A and GO-06549.01-95A for work that is related to data from HST.

REFERENCES

- Clowe, D., Luppino, G.A., Kaiser, N., & Gioia, I.M. 2000, *ApJ*, 539, 540
- Hoekstra, H., Franx, M., Kuijken, K., & Squires, G. 1998, *ApJ*, 504, 636
- King, I.R. 1971, *PASP*, 83, 199
- Krist, J.E. in *Calibrating Hubble Space Telescope, Post Servicing Mission*; eds. A. Koratkar & C. Leitherer; Proceedings of a Workshop held at Space Telescope Science Institute, Baltimore 1995 (STScI; Baltimore)
- Lauer, T. 1985, *ApJS*, 57, 473
- Lubin, L.M., Postman, M., Oke, J.B., Ratnatunga, K.U., Gunn, J.E., Hoessel, J.G., & Schneider, D.P. 1998, *AJ*, 116, 584
- Lubin, L.M., Postman, M., Oke, J.B., Brunner, R., Gunn, J.E., & Schneider, D.P. 2001, *AJ*, in preparation
- Lubin, L.M., & Sandage, A. 2001a, *AJ*, in preparation (Paper III)
- Lubin, L.M., & Sandage, A. 2001b, *AJ*, in preparation (Paper IV)
- Oke et al. 1995, *PASP*, 107, 375
- Oke, J.B., Postman, M., & Lubin, L.M. 1998, *AJ*, 116, 549
- Petrosian, V. 1976, *ApJ*, 209, L1
- Postman, M. & Lauer, T. 1995, *ApJ*, 440, 28
- Postman, M., Lubin, L.M., & Oke, J.B. 1998, *AJ*, 116, 560
- Postman, M., Lubin, L.M., & Oke, J.B. 2001, *AJ*, in preparation
- Saglia, R.P., Bertschinger, E., Baggle, G., Burstein, D., Colless, M., Davies, R.L., McMahan, R.K., & Wegner, G. 1993, *MNRAS*, 264, 961
- Sandage, A. 1972a, *ApJ*, 173, 485
- Sandage, A. 1972b, *ApJ*, 178, 1
- Sandage, A. 1972c, *ApJ*, 178, 25
- Sandage, A. 1973, *ApJ*, 183, 711
- Sandage, A., & Lubin, L.M. 2001, *AJ*, submitted (Paper I)
- Sandage, A., & Perelmuter, J-M. 1990, *ApJ*, 361, 1

- Sandage, A., & Perelmuter, J-M. 1991, ApJ, 370, 455
- Schweizer, F. 1979, ApJ, 233, 23
- Schweizer, F. 1981, AJ, 86, 662
- Sparks, W.B. 1988, AJ, 95, 1569
- Squires, G.K. et al. 2001, ApJ, in preparation
- Watanabe, M., Kodaira, K., & Okamura, S. 1982, ApJS, 50, 1

Fig. 1.— The effect of various point spread functions and/or seeing disks on the photometric parameters for a galaxy with an effective (half-light) radius of $0''.70$. The curves in each panel are derived from a synthetic galaxy which has a de Vaucouleurs $r^{\frac{1}{4}}$ profile and is circularly symmetric. The three panels show the surface brightness profile (upper left), the Petrosian η function (upper right), and the growth curve of the total magnitude within a given radius r (lower left), all as a function of $\log r$ where r is in arcsec. The normalizations of the ordinates for the surface brightness and total magnitude profile are from the actual data for the galaxy HST #9 in the cluster Cl 1324+3011 ($z = 0.76$) as given in Paper III. The solid red line in each panel indicate the intrinsic relation for zero seeing, while the remaining three lines indicate the relations with Gaussian seeing of $0''.1$ (blue dots), $0''.3$ (magenta short dashes), and $0''.9$ (cyan long dashes), respectively.

Fig. 2.— Same three panels as Figure 1, but for a simulated galaxy of half-light radius $0''.25$ which closely resembles galaxy HST #59 in Cl 1324+3011.

Fig. 3.— Same panels as given in Figures 1 and 2, but using actual observations of the galaxy HST #18 in Cl 1324+3011 made with both the *Hubble Space Telescope* (solid circles) and the Keck 10-m ground-based telescopes (open circles). The bandpass is the Cape/Cousins I band for the Keck data and the F814W filter for the HST data, respectively (see §3).

Fig. 4.— Same panels as Figure 3, but using actual observations of the galaxy HST #40 in Cl 1324+3011 made with both HST and the Keck telescopes.

Fig. 5.— Same panels as in Figures 3 and 4, but for the galaxy HST #69 in Cl 1324+3011 that was observed both with HST and the Keck telescopes. This galaxy is the smallest of the three galaxies which are presented in Figures 3–5.

Fig. 6.— CCD image of the galaxy HST #11 in the cluster Cl 1324+3011 taken from the full WFPC2 image of a 32.0 ksec observation in the F814W filter. The image is $5'' \times 5''$.

Fig. 7.— Same as Figure 6, but for the highly elongated elliptical galaxy HST #12 in Cl 1324+3011.

Fig. 8.— The difference in the photometric correlations using the three methods discussed in §4 for reducing the two-dimensional intensity data. The four panels show the surface brightness (upper left), Petrosian η function (upper right), and growth curve (lower left) as a function of radius (either circular radius, semi-major axis, or \sqrt{ab}) in arcsec, and the mean surface brightness as a function of η (lower right). The curves are derived from data taken with HST for the galaxy HST #11 in Cl 1324+3011. The solid blue circles, solid cyan squares, and open red circles indicate the circular aperture, elliptical aperture, and \sqrt{ab} methods, respectively (see §4.2).

Fig. 9.— Same four panels as Figure 8, but for the highly elongated elliptical galaxy HST #12 in Cl 1324+3011.

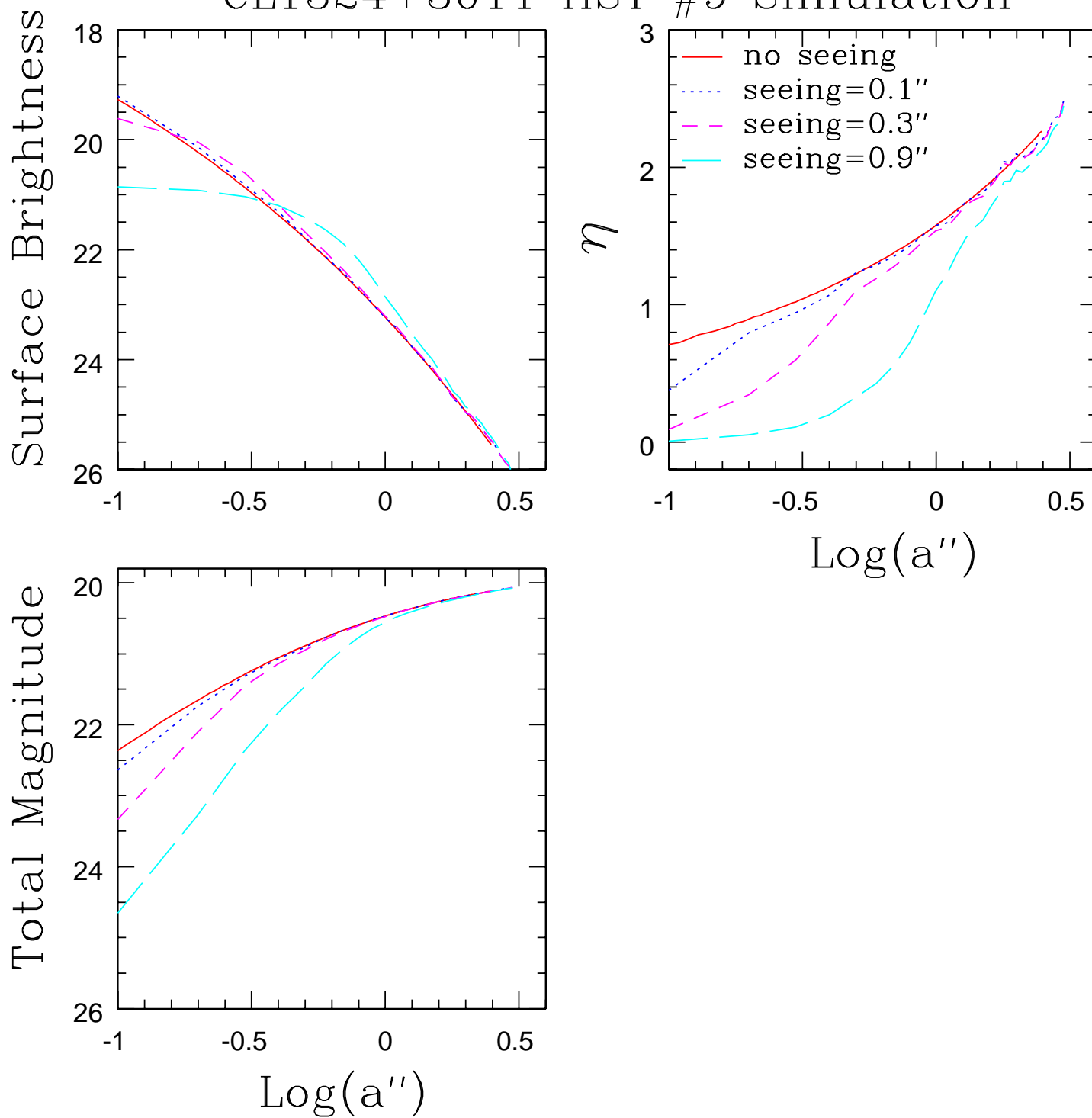
Table 1. Properties of the Galaxies from Cl 1324+3011 used in the HST versus Keck Comparison

HST # ^a	Class ^a	m_{814} ^a	r_{eff} ^a	B ^b	V ^b	R ^b	I ^b	z
18	E/S0	20.85	0.35	25.25	23.38	22.14	20.88	0.7592
40	E	21.69	0.26	25.91	23.98	23.22	21.60	0.7618
69	S0	22.26	0.17	...	24.29	23.89	22.20	0.7628

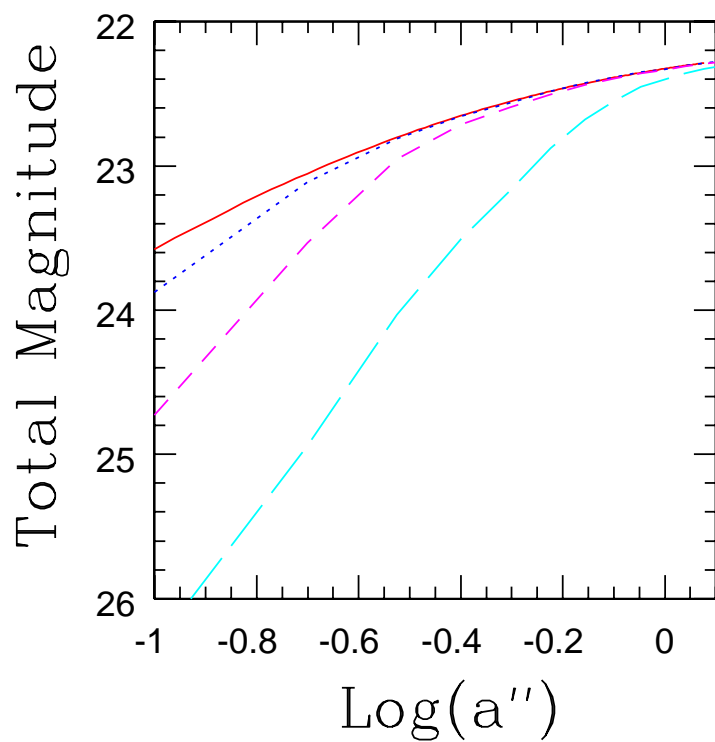
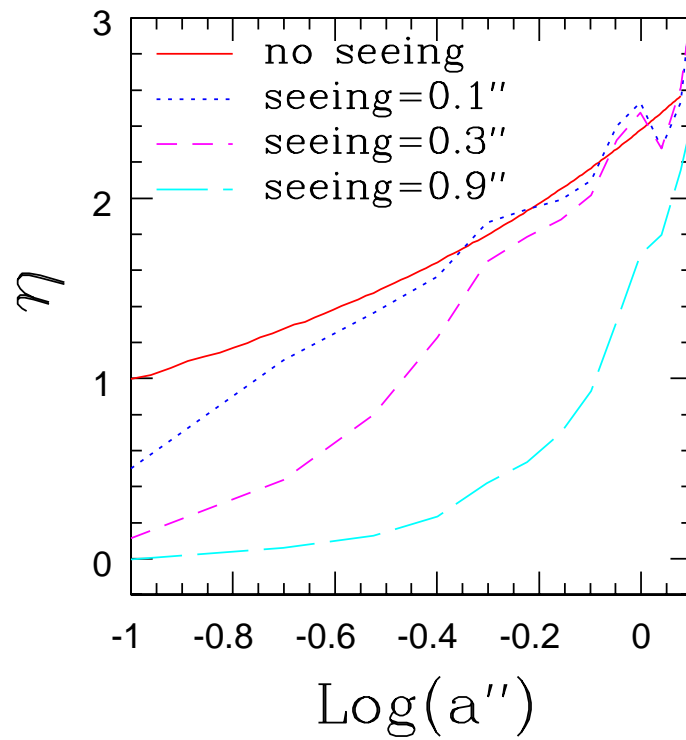
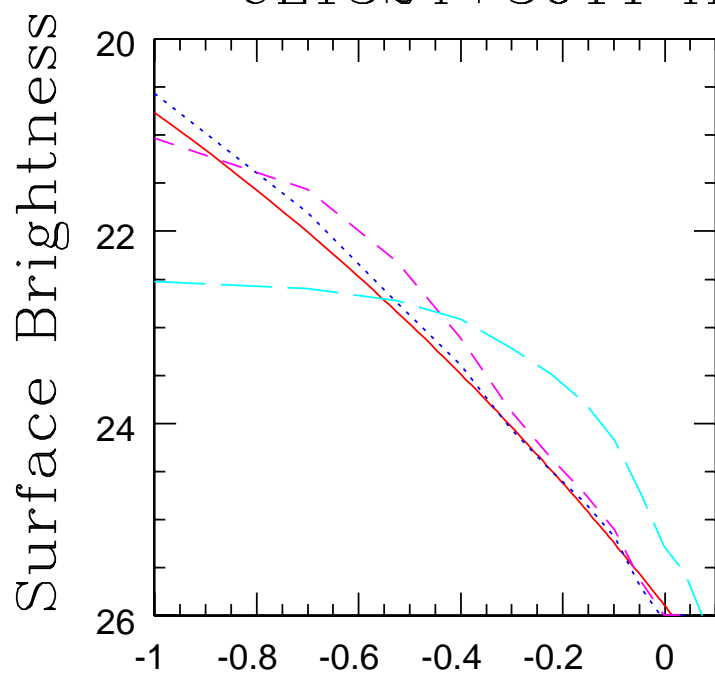
^aThe identification number, visual morphological classification, total galaxy magnitude, and effective radius (in arcsec) of the galaxy surface brightness profile as measured from the WFPC2 image taken in the F814W filter (see Lubin et al. 2001).

^bKeck $BVRI$ photometry computed in a circular aperture with radius of 3'' (see Postman, Lubin & Oke 2001).

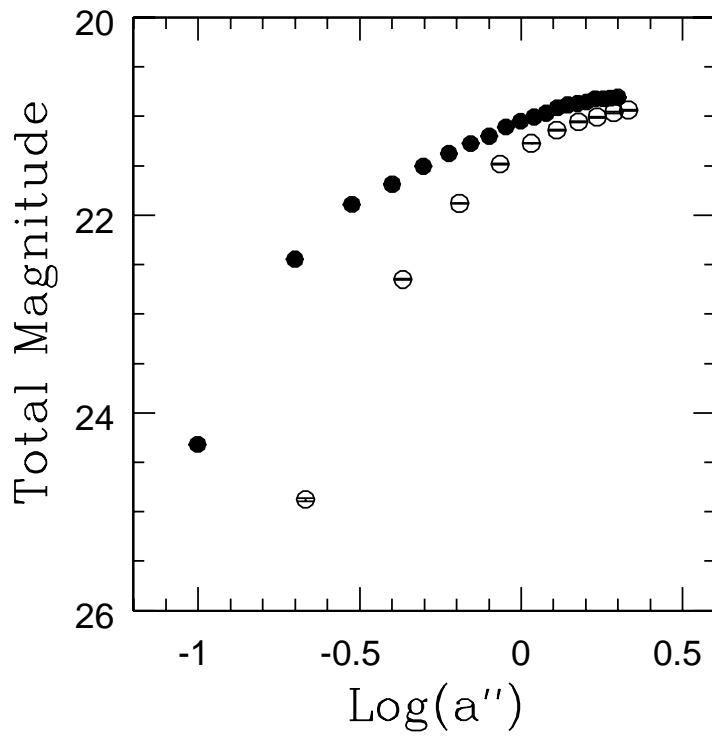
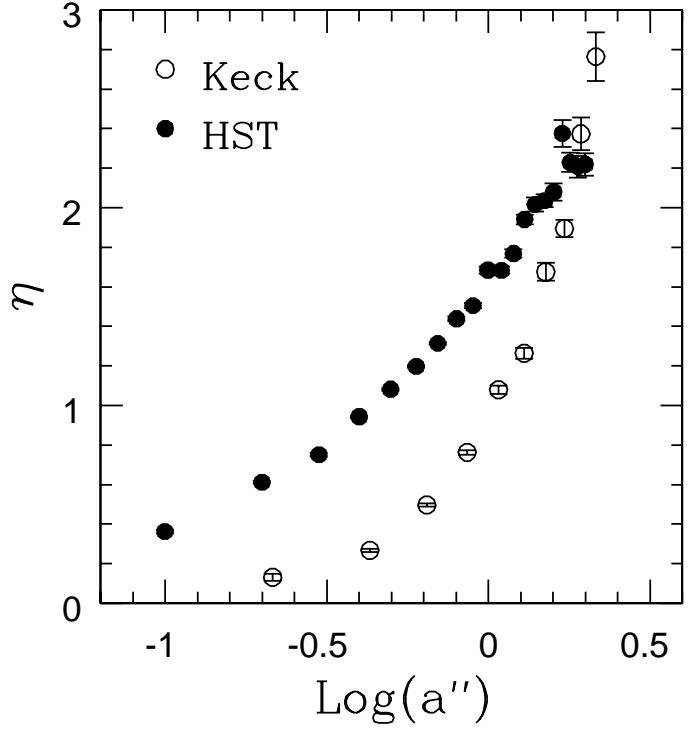
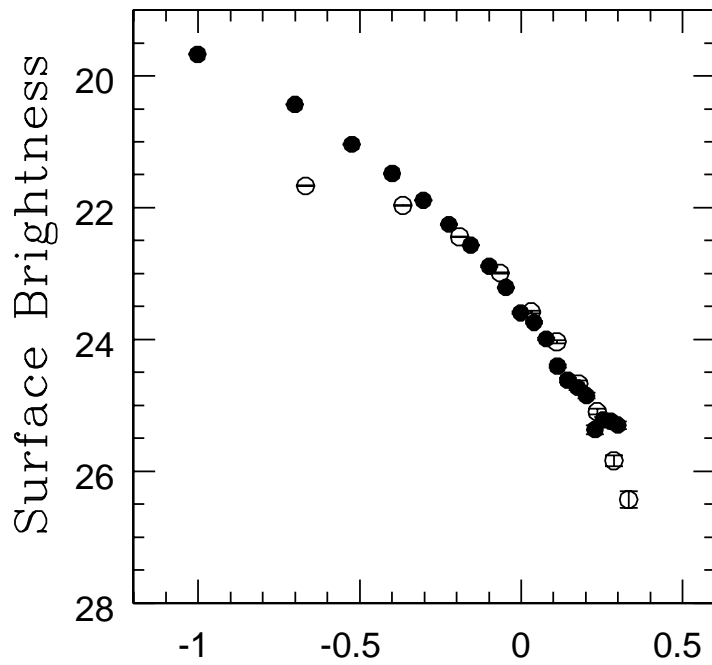
CL1324+3011 HST #9 Simulation



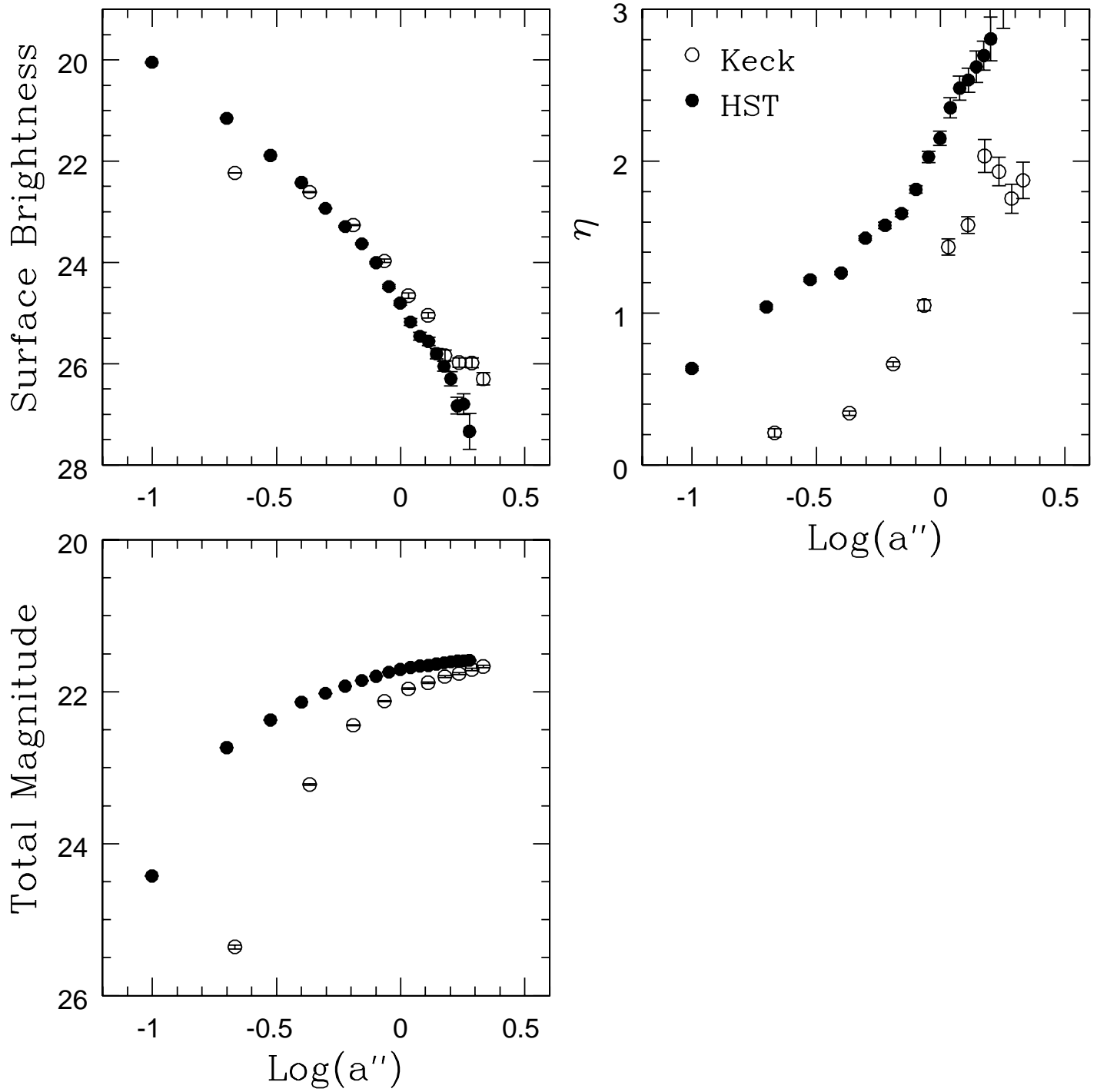
CL1324+3011 HST #59 Simulation



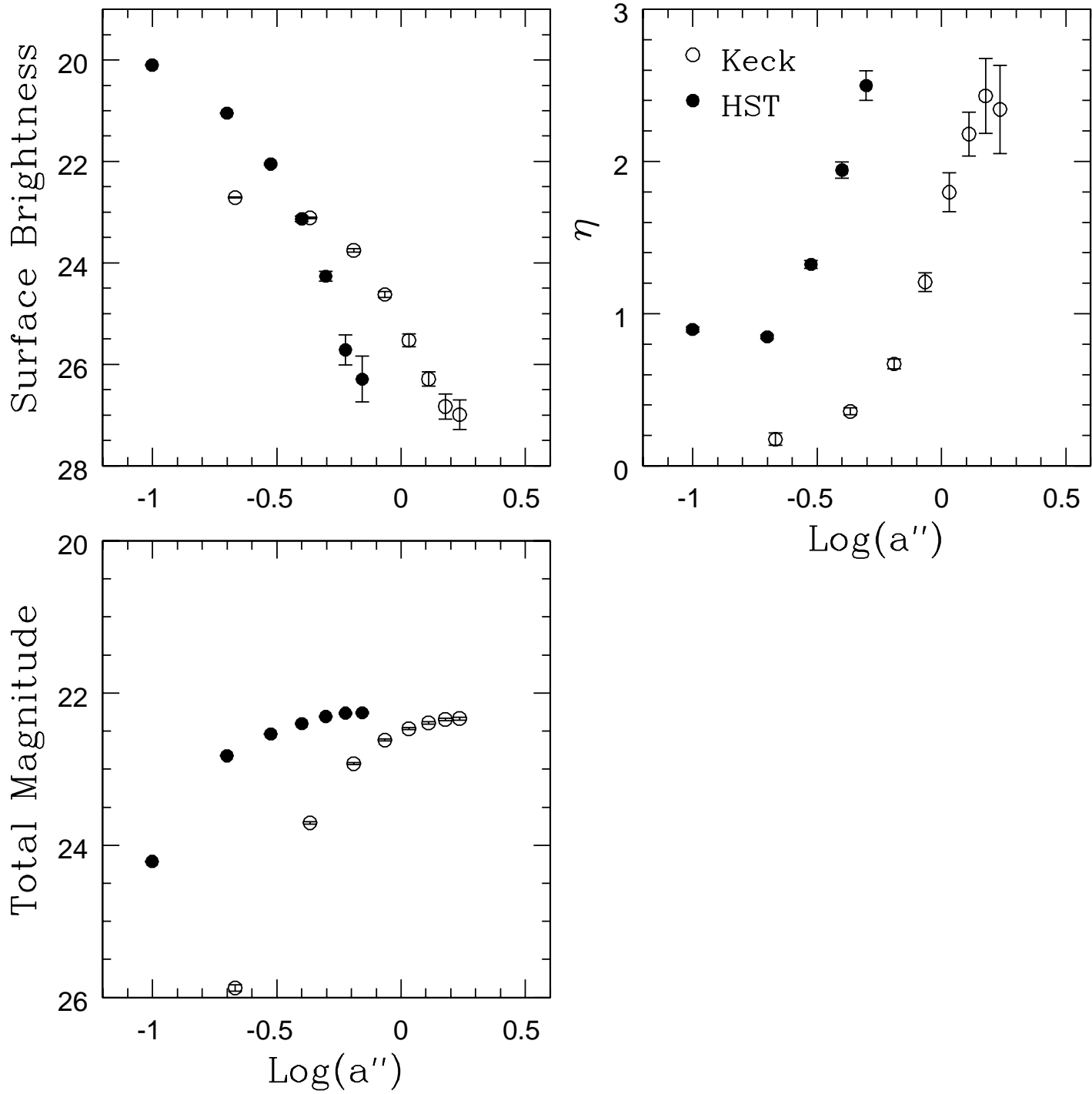
CL1324+3011 HST #18 Comparison



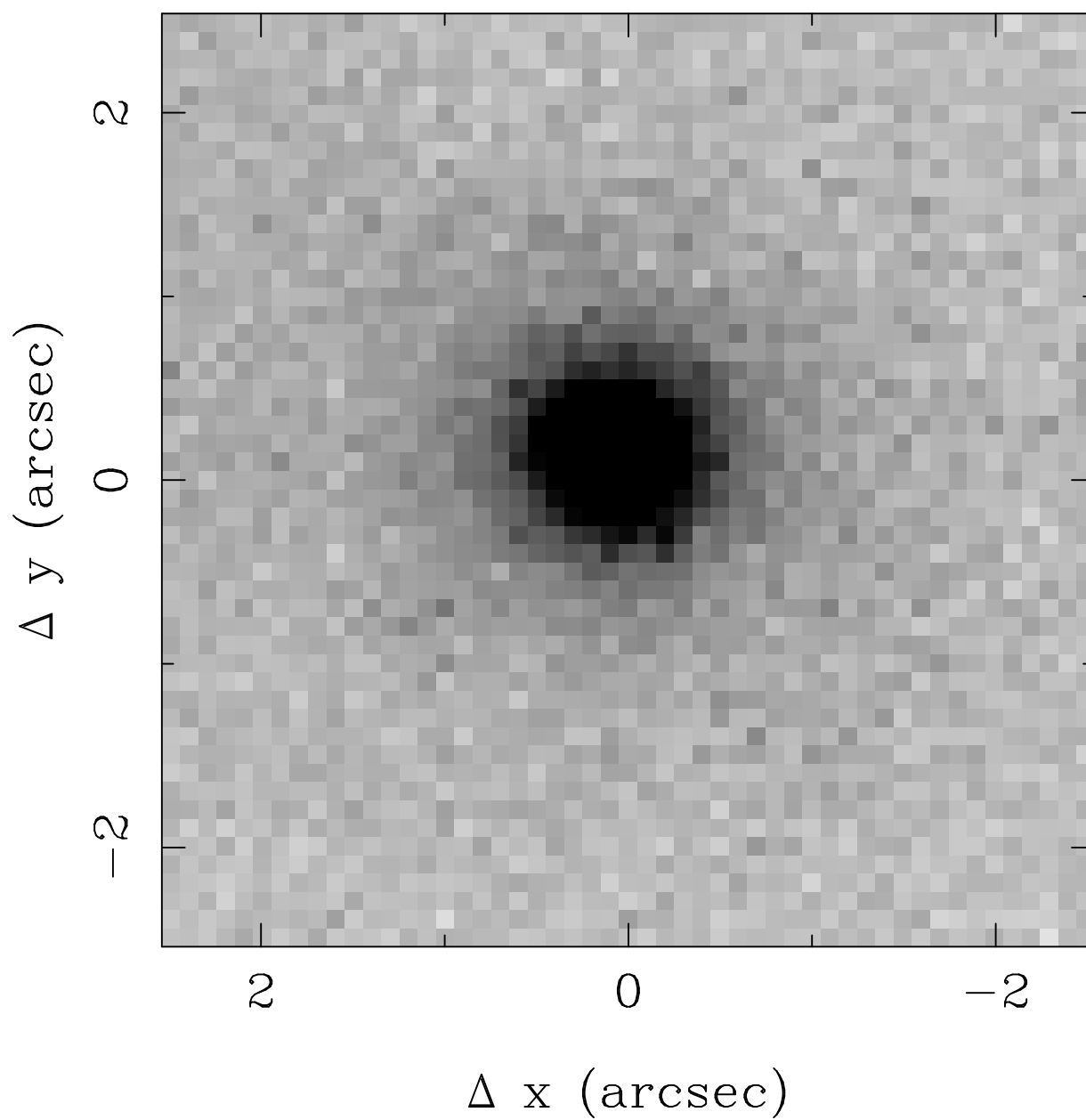
CL1324+3011 HST #40 Comparison



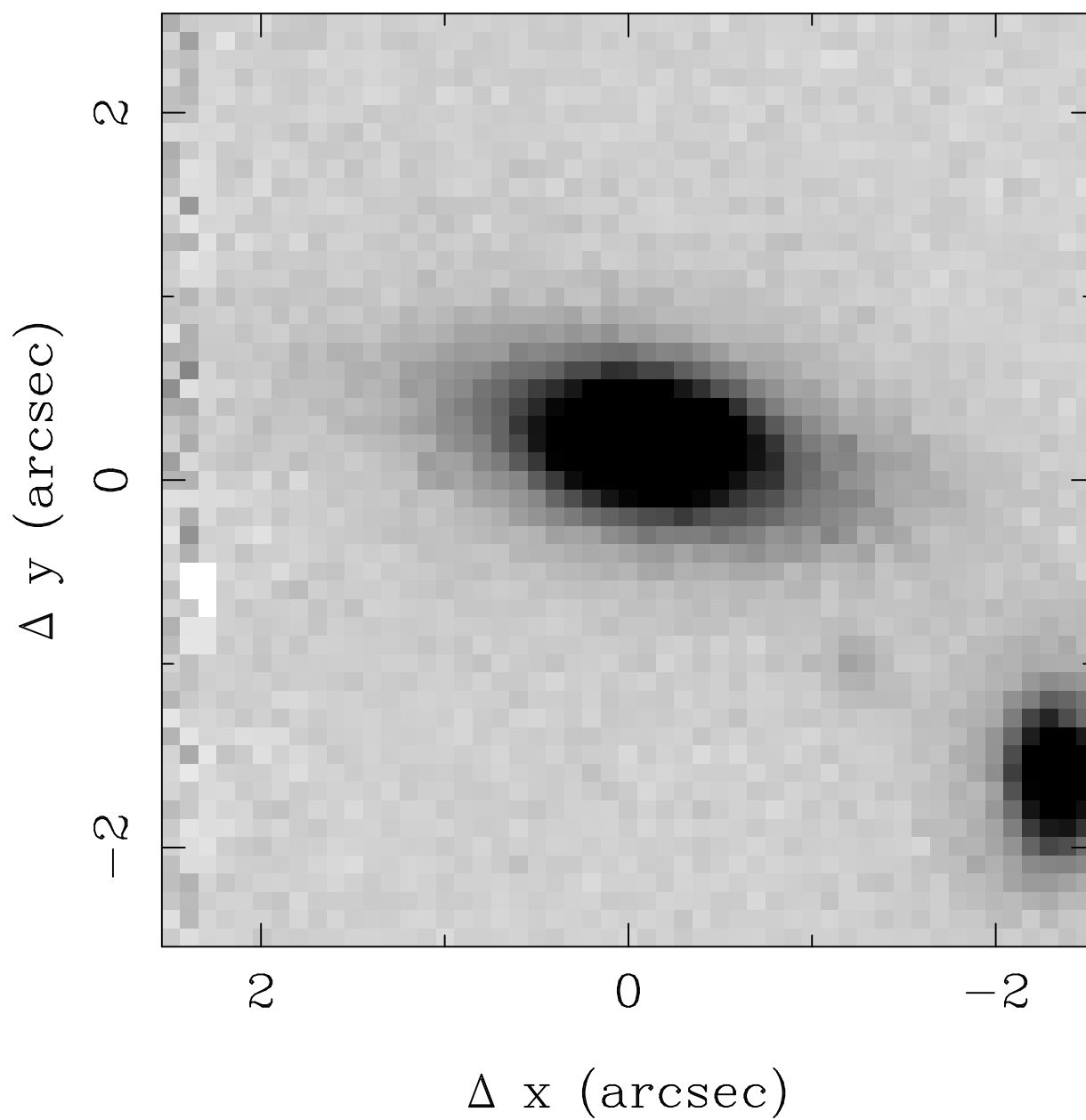
CL1324+3011 HST #69 Comparison



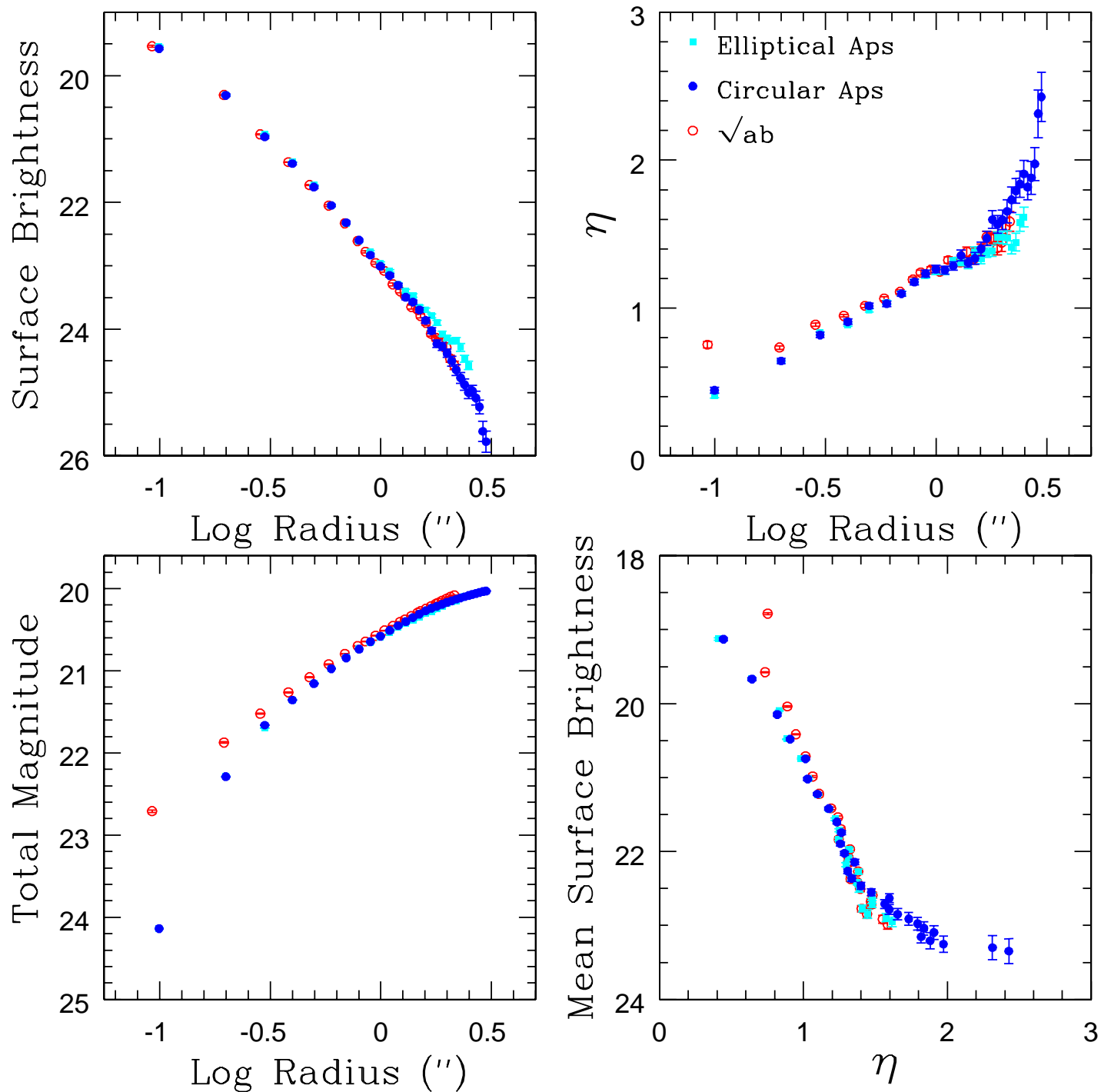
CL1324+3011 HST #11



CL1324+3011 HST #12



CL1324+3011 HST # 11



CL1324+3011 HST # 12

